Whirl-Flutter Investigation on an Advanced Turboprop Configuration

F. Nitzsche*
EMBRAER—Empresa Brasileira de Aeronáutica S.A., São José dos Campos, Brazil

The whirl-flutter problem of an advanced turboprop configuration with two pusher propellers positioned at the aircraft fuselage cone is analyzed. Coupling between the two propellers and the flexible backup structure—pylons and aft fuselage cone—is allowed. Very interesting results lead to the conclusion that, for typical stiffness ratios between the backup structure and the engine suspension system, a special type of flutter involving mainly the backup structure may be dominant over traditional propeller-nacelle whirl flutter. This type of flutter is solely due to the propeller whirl and may be critical either in some modern configurations of aircrafts (as propfans) or in new conceptions of power plants installations employing additional vibration insulators at the pylon-fuselage attachments.

Nomenclature

$\boldsymbol{A},\boldsymbol{B}$ = eigenvalue problem matrices (dimensionless)
$A_1, \ldots, A_3$ = aerodynamic influence coefficients
a = distance between fuselage and nacelle centerlines
a_0 = lift-curve slope
b = engine-propeller c.g. distance from pylon elastic axis
C = $4N\Omega^2R^2m_a/c_0^2$
c, c_0 = blade chord, blade reference chord
d = propeller distance from pylon elastic axis
E = potential energy
$\boldsymbol{e}_{L_\pm}$ = unit vector in the direction of $\boldsymbol{L}$
$\boldsymbol{e}_{r_\pm}, \boldsymbol{e}_{\Omega_\pm}, \boldsymbol{e}_{x_\pm}$ = triad defines x_0-aligned, blade-fixed rotating frame
$\boldsymbol{e}''_{r_\pm}, \boldsymbol{e}''_{\Omega_\pm}, \boldsymbol{e}''_{x_\pm}$ = triad defines x''-aligned, blade-fixed rotating frame
f_a, f_b = Eqs. (18a) and (18b)
$\boldsymbol{G}$ = gyroscopic matrix (dimensionless)
h = pylon elastic axis out-of-plane displacement
h_y, h_z = aft fuselage cone displacement: horizontal, vertical
J/π = $V/\Omega R$
$\boldsymbol{K}$ = stiffness matrix (dimensionless)
k_a = k_ψ/k_ϕ (Fig. 2)
k_1 = k_v/k_w (Fig. 2)
L = lift perturbation
L_{y_0}, L_{z_0} = lift components along y_0 and z_0
$\mathcal{L}$ = Laplace transform
M = aerodynamic-moment perturbation
$\boldsymbol{M}$ = mass matrix (dimensionless)
M_{y_0}, M_{z_0} = aerodynamic-moment components about y and z_0
M_0, m_0 = fuselage, nacelle mass
m_a = $\rho(\pi c_0^2/4)R$
m_e, m_h = engine, propeller mass
N = number of blades
Q_i = generalized forces
$\boldsymbol{Q}^0, \boldsymbol{Q}^1$ = aerodynamic stiffness, aerodynamic damping matrices (dimensionless)
q_i = generalized coordinates
R = propeller radius
r = blade-section radial coordinate
s = perturbation along Ωr
T = kinetic energy
t = time
U = blade-section resultant velocity
u = perturbation along V
u_ψ, u_η = components of u: yaw, pitch
V = undisturbed airspeed
v = horizontal displacement of the engine c.g. relative to the nacelle
W = virtual work done by the aerodynamic forces
w = vertical displacment of the engine c.g. relative to the nacelle
X, Y, Z = inertial frame
x, y, z = nacelle-fixed reference frame
x_0, y_0, z_0 = aft fuselage cone-fixed reference frame
x', y', z' = engine-propeller reference frame after pitch rotation
x'', y'', z'' = engine-propeller reference frame after pitch and yaw rotations
y_r, z_r = perturbations along y and z (Fig. 4)
β, β' = velocity diagram resultant angles (Fig. 7)
γ = pylon rotation about the elastic axis
$\Delta\alpha, \Delta\alpha_a, \Delta\alpha_v$ = blade-section angle-of-attack perturbations: total, angular-displacement, induced-velocity components
η = $-(\gamma+\phi)$
θ = aft fuselage cone rotation about the aircraft centerline
μ = $2N\bar{m}_a/\bar{c}_0$
ρ = air density
ϕ = engine-propeller pitch displacement
ψ = engine-propeller yaw displacement
ω = aeroelastic-mode frequency
ω_i = engine-propeller uncoupled natural frequencies ($i = v, w, \psi, \phi$)
$\omega_y, \omega_z, \omega_\theta$ = aft fuselages cone uncoupled natural frequencies
$\omega_\delta, \omega_\gamma$ = pylon uncoupled natural frequencies
$\Omega_\pm$ = propeller spinning frequency (clockwise/counterclockwise)
$\mathbf{1}, \mathbf{0}$ = unit, null matrices (null vector)

Superscripts

$\cdot$ = time differentiation
$*$ = $1/\Omega\ \partial/\partial t$
$\hat{}$ = Laplace-transformed vector

Presented as Paper 88-2346 at the AIAA/ASME/ASCE/AHS 29th Structures, Structural Dynamics, and Materials Conference, Williamsburg, VA, April 18-20, 1988; received June 20, 1988; revision received March 21, 1989.

*Manager's Assistant, Advanced Methods Group; also, Visiting Professor, Instituto Tecnológico de Aeronáutica. Member AIAA.

$\bar{}$ = dimensionless value
T = transpose matrix

Subscripts

$\pm$ = clockwise ($\Omega>0$), counterclockwise ($\Omega<0$)
1,2 = referred to power plants 1,2
I = transpose matrix

Introduction

THE whirl flutter has for long been recognized as a major aeroelastic problem related to turboprop-powered aircrafts. The introduction of such phenomenon in the literature is historically due to Taylor and Browne as early as 1938.[1] However, its importance remained academic until the 1960s when two fatal flight accidents were linked to whirl-flutter onset. Since then, several works appeared in the literature.[2-8]

The present paper is focused on the whirl-flutter problem applied to a new advanced turboprop configuration of airplane, in which two pusher engines are supported by short pylons cantilevered with the aft fuselage cone. This problem will prove to be extremely interesting as long as a dynamic coupling involving the two propellers and the flexible backup structure is observed.

System Dynamics

Two-degree-of-freedom (pitch-yaw) models, such as those originally introduced by Reed and Bland[2] and Houbolt and Reed,[3] are able to reproduce the precessional motion of the propeller relative to the nacelle, which may become unstable under certain circumstances.

Nevertheless, more sophisticated idealizations incorporating more degrees of freedom, particularly those associated with the lateral motion of the power plant center of mass relative to the nacelle, have indicated that the pitch-yaw model is not always representative.[7] In another work, Zwaan and Bergh[4] demonstrated that a flexible backup structure, namely the wing on which the power plants are installed, significantly modifies the dynamic behavior of the system.

A sketch of the relatively simple model used in the present analysis is shown in Fig. 1. In order to incorporate only the essential degrees of freedom necessary to a reliable whirl-flutter study, both the fore-and-aft and torsion degrees of freedom of the propeller relative to the nacelle are skipped once they were already recognized to have little importance on the critical aeroelastic modes.[7,9] Springs mathematically idealize the flexibilities of the aft fuselage cone (lateral and torsion) and pylons (bending and torsion). No damping is introduced in the system.

Mass and mass moment of inertia of each element of the system are properly concentrated at the respective c.g. position. Such a lumping procedure is expected to provide fairly good results, since it allows further adjustments for both the spring stiffness rates and mass properties to match the frequencies and the generalized masses of the backup structure uncoupled natural modes. In a more rigorous approach, the diagonal stiffness matrix, as obtained by means of the aforementioned technique, may be substituted by a full matrix of structural influence coefficients. Higher backup structure modes are assumed to play no role on the whirl-flutter stability.

In Fig. 2, the engine-nacelle suspension system is represented by its global characteristics. The engine is assumed to be a rigid body free to move in pitch, yaw, and in the vertical and horizontal directions.

Energy methods are used to obtain the linear differential equations describing the system dynamics. Eight auxiliary reference axes are defined in Fig. 3 as follows: 1) X-Y-Z inertial is fixed to a rigid point of the aircraft, for example, the wing main spar; 2) x_0-y_0-z_0 is defined by the aft fuselage cone displacements: h_y along Y, h_z along Z, and a positive rotation θ about X; 3) x_1-y_1-z_1; 4) x_2-y_2-z_2 are aligned with the nacelle centerlines (distance a from the fuselage centerline) and defined by both the out-of-plane bending displacements of the pylon ends (h_1 and h_2, positive downwards) and the associated torsions (γ_1 and γ_2, positive rotations about y_0); 5) x_1'-y_1'-z_1'; 6) x_2'-y_2'-z_2' are defined by the lateral displacements of the engine-propeller c.g. (w_1 and w_2 along z_1 and z_2, and v_1 and v_2 along y_1 and y_2) and positive pitch rotations (ϕ_1 and ϕ_2 about y_1 and y_2); 7) x_1''-y_1''-z_1''; and 8) x_2''-y_2''-z_2'', defined by positive yaw rotations (ψ_1 and ψ_2 about z_1' and z_2'). Therefore, after the perturbations, the propellers are aligned with x_1'' and x_2''. The airplane flies along the negative X axis, so that the air velocity vector V is as indicated in Fig. 3. Positive, clockwise,

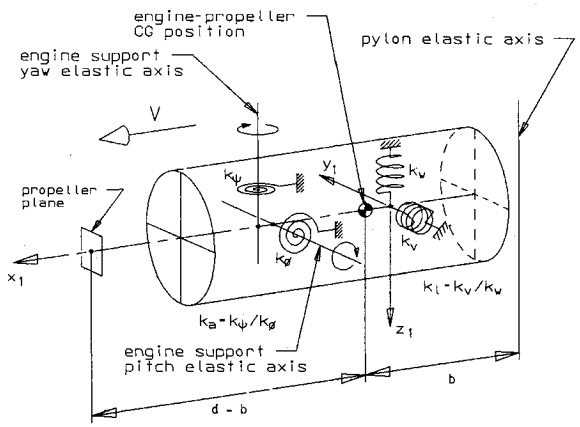

Fig. 2 Engine-suspension system characteristics.

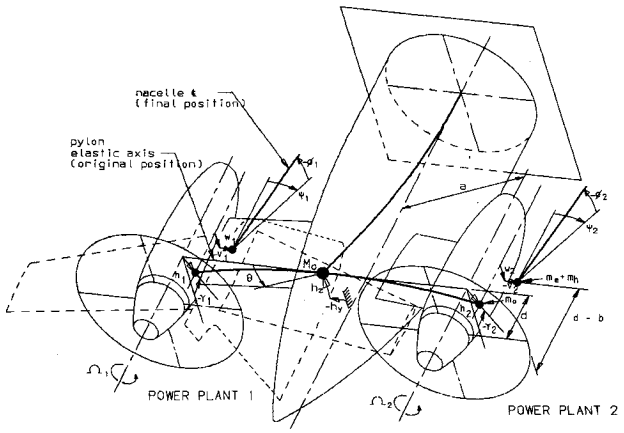

Fig. 1 Fifteen-degree-of-freedom model.

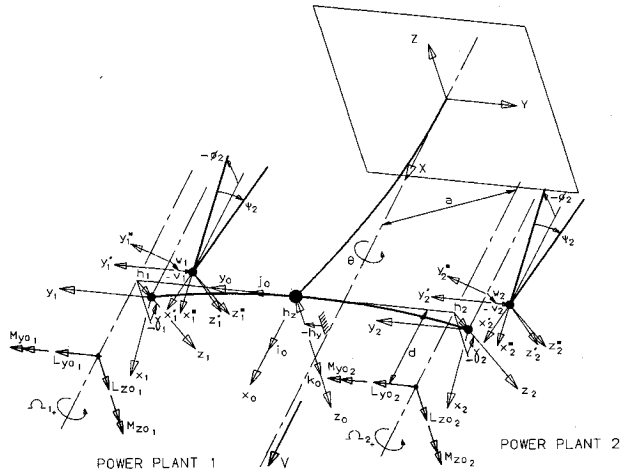

Fig. 3 Reference frames and generalized forces definition.

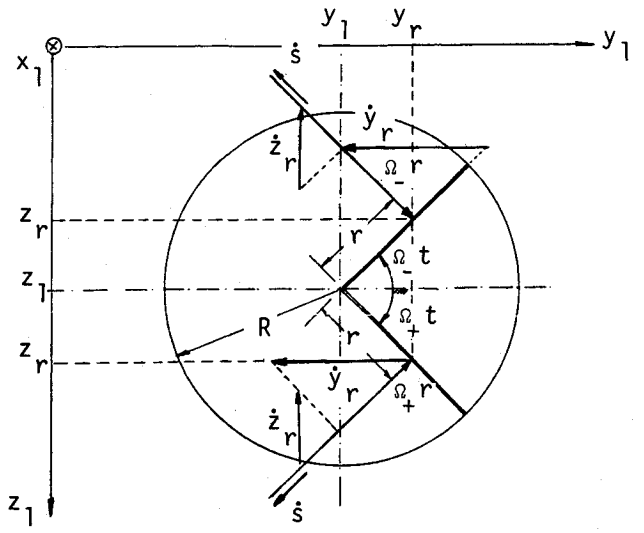

Fig. 4 In-plane perturbations.

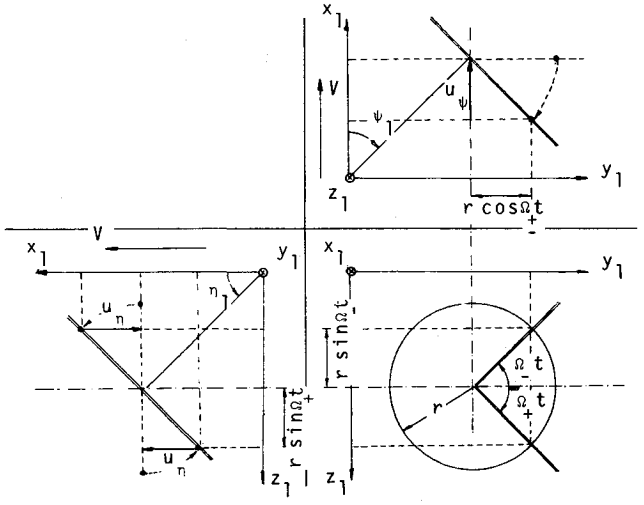

Fig. 5 Out-of-plane perturbations.

propeller rotations are in agreement with positive rotations about x_1'' and x_2''.

Propeller Aerodynamics

The present whirl-flutter model considers a two-dimensional, unsteady, small-perturbation aerodynamics. A lift-curve slope correction for compressibility may be introduced. A basis is Houbolt and Reed's aerodynamic model developed in their two-degree-of-freedom whirl-flutter investigation.[3] It is reviewed here and extended to allow for the analysis of propellers rotating either clockwise or counterclockwise, subject not only to pitch and yaw motions, but also to the lateral motion due to the power plant c.g. displacement relative to the nacelle. The contribution from the backup structure motion to the velocity induced at the propeller disk is taken into account as well. The perturbation flowfield caused by the presence of the back up structure is not modeled.

Velocity Perturbation

In-Plane Contribution

The propeller disk is displayed in Fig. 4. The position of a point on a blade section distance r from the hub is given by

$$y_r = y_{1,2} + r\cos\Omega_{\pm}t \tag{1}$$

$$z_r = z_{1,2} \pm r\sin\Omega_{\pm}t \tag{2}$$

where, in the expression for z_r, the upper sign corresponds to the positive clockwise and the lower sign to the negative counterclockwise propeller spinning direction. This convention is maintained throughout the paper, unless otherwise specified.

Assuming that the induced airspeed $\dot{s}$ is positive against the tangential airspeed Ωr, from Fig. 4 one has

$$\dot{s} = \dot{y}_r\sin\Omega_{\pm}t \mp \dot{z}_r\cos\Omega_{\pm}t + \Omega_{\pm}r \tag{3}$$

Substituting Eqs. (1) and (2) into Eq. (3),

$$\dot{s} = \dot{y}_{1,2}\sin\Omega_{\pm}t \mp \dot{z}_{1,2}\cos\Omega_{\pm}t \tag{4}$$

Out-of-Plane Contribution

Figure 5 shows the out-of-plane displacement vector of a point lying on the blade when positive rotations about z_1 and y_1 are undergone by the propeller hub. The positive displacements are assumed against the normal airspeed V. Under the small-angle assumption,

$$u_\psi = -\psi_{1,2}r\cos\Omega_{\pm}t \tag{5}$$

$$u_\eta = \mp\eta_{1,2}r\sin\Omega_{\pm}t \tag{6}$$

where

$$\eta_{1,2} = -\phi_{1,2} - \gamma_{1,2} \tag{7}$$

is the total pitch displacement due to both the power plant motion in the nacelle and the pylon torsion. In order to obtain the overall out-of-plane perturbation, it will suffice to sum the two components of u:

$$u = u_\psi + u_\eta \tag{8}$$

The induced out-of-plane airspeed is readily obtained by differentiating u with respect to time, yielding

$$\dot{u} = r[(-\dot{\psi}_{1,2} \mp \eta_{1,2}\Omega_{\pm})\cos\Omega_{\pm}t + (\mp\dot{\eta}_{1,2} + \psi_{1,2}\Omega_{\pm})\sin\Omega_{\pm}t] \tag{9}$$

It is worth observing in Eq. (9) that there are two distinct contributions to the out-of-plane induced velocity; namely, 1) the contribution from an angular speed about y_1 and z_1, and 2) the contribution from an angular displacement about the same y_1 and z_2, which when combined with the propeller rotation makes a point on a blade element to describe a fore-and-aft cyclical motion with the propeller frequency.

Angular Perturbation

Angular deflections of the propeller hub relative to the undisturbed airstream generate variations on the blade angle of attack. These can be estimated by defining two additional reference frames: the first is aligned with the x_0 axis, and so with the undisturbed airspeed vector V; and the second is pointing towards the x'' axis. They are both rotating either clockwise or counterclockwise with the propeller blades, according to Fig. 6. The change in the blade angle of attack due to positive angular deflections of the propeller hub is hence obtained:

$$\Delta\alpha_a = |e_{\Omega_{\pm}}'' - e_{\Omega_{\pm}}|/|e_{\Omega_{\pm}}''| \tag{10}$$

which, after some straightforward algebra,[10] yields

$$\Delta\alpha_a = \psi_{1,2}\sin\Omega_{\pm}t \mp \eta_{1,2}\cos\Omega\pm t \tag{11}$$

Blade Angle of Attack: Clockwise/Counterclockwise

The velocity diagrams for a propeller blade section and the two studied configurations represented by the clockwise and

the counterclockwise propeller rotations are depicted in Fig. 7.

Under the sign convention adopted for $\dot{s}$ and $\dot{u}$, an increase in the blade angle of attack due to the induced velocities is given by

$$\Delta\alpha_v = \beta - \beta' \simeq \tan(\beta - \beta') \tag{12}$$

where

$$\tan\beta = V/\Omega R, \qquad \tan\beta' = (V - \dot{u})/(\Omega r - \dot{s}) \tag{13}$$

Breaking the tangent of the difference into its components and linearizing the result, an expression for $\Delta\alpha_v$ is obtained in terms of $\dot{s}$ and $\dot{u}$:

$$\Delta\alpha_v = \dot{u}(\Omega r/U^2) - \dot{s}(V/U^2) \tag{14}$$

The total change in the blade angle of attack is the difference between the two incremental angles:

$$\Delta\alpha = \Delta\alpha_v - \Delta\alpha_a \tag{15}$$

since $\Delta\alpha_a$ is determined by a blade displacement in the $x_{1,2}''$ direction, which decreases the angle of attack. In simpler words, the contribution to $\Delta\alpha$ due to $\Delta\alpha_v$ is given by a perturbation in the velocity diagram generated by $\dot{u}$ and $\dot{s}$, whereas the contribution to $\Delta\alpha$ due to $\Delta\alpha_a$ is provided by a blade-section rotation with respect to the "fixed" velocity diagram, which justifies the minus sign in Eq. (15).

Propeller Thrust and Aerodynamic Moment

According to the strip-theory assumption,

$$\partial L/\partial r = (a_0/2)\rho c U^2 \tag{16}$$

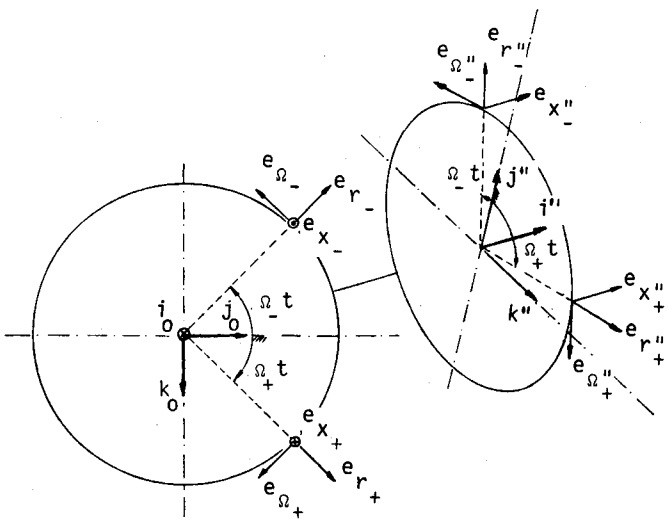

Fig. 6 Blade-fixed reference frames.

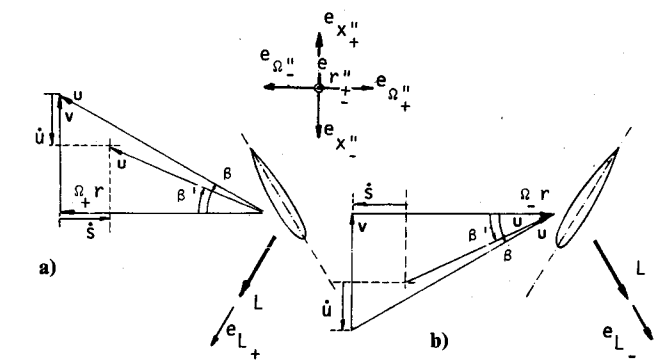

Fig. 7 Blade-section velocity diagrams: a) clockwise rotation, and b) counterclockwise rotation.

which leads to

$$\partial L/\partial r = f_a \cos\Omega_\pm t + f_b \sin\Omega_\pm t \tag{17}$$

where, assuming for simplicity $a_0 = 2\pi$,

$$f_a = -\pi\rho c(\Omega_\pm r^2\dot{\psi}_{1,2} \mp V\dot{z}_{1,2} \mp V^2\eta_{1,2}) \tag{18a}$$

$$f_b = \pi\rho c(\mp\Omega_\pm r^2\dot{\eta}_{1,2} - V\dot{y}_{1,2} - V^2\psi_{1,2}) \tag{18b}$$

Since,

$$\partial L/\partial r = \partial L/\partial r e_{L_\pm} \tag{19}$$

and from Fig. 7

$$e_{L_\pm} = \mp e_{x_\pm}'' \cos\beta - e_{\Omega_\pm}'' \sin\beta \tag{20}$$

the lift-vector perturbation per unit of blade span is calculated[10]

$$\partial L/\partial r = \partial L/\partial r(\sin\Omega_\pm t\, j_0 \mp \cos\Omega_\pm t\, k_0)\ V/U \tag{21}$$

In addition, by taking the crossproduct between the radial and the lift vectors, the aerodynamic moment per unit of blade span is obtained[10]

$$\partial M/\partial r = r\, e_{r_\pm}'' \times \partial L/\partial r$$

$$= r\partial L/\partial r(\mp \sin\Omega_\pm t\, j_0 + \cos\Omega_\pm t\, k_0)\ \Omega r/U \tag{22}$$

Summing up the contribution from the N blades and applying the dot product in the j_0 and k_0 directions, the y_0 and z_0 components of both the lift and the aerodynamic moment perturbations per unit of blade span are computed

$$\partial L/\partial r = (N/2)(f_b j_0 \mp f_a k_0)\ V/U \tag{23a}$$

$$\partial M/\partial r = (N/2)(\mp f_b j_0 + f_a k_0)\ \Omega r^2/U \tag{23b}$$

which is valid either for a pusher or a tractor propeller.

It is worth observing that the $\Omega_\pm t$ dependence cancels out in the summing procedure, whatever the number of blades might be, remaining solely the dependence on N.[10] An integration along the blade span leads to the final result for both the lift (or thrust) and the aerodynamic moment developed by the propeller

$$L_{y_0} = C[-(c_0/2)A_1'\psi_{1,2} - (c_0/2\Omega R)A_1\dot{y}_{1,2}$$

$$\mp (c_0 R/2\Omega R)A_2\dot{\eta}_{1,2}] \tag{24a}$$

$$L_{z_0} = C[-(c_0/2)A_1'\eta_{1,2} - (c_0/2\Omega R)A_1\dot{z}_{1,2}$$

$$\pm (c_0 R/2\Omega R)A_2\dot{\psi}_{1,2}] \tag{24b}$$

$$M_{y_0} = RC[\pm(c_0/2)A_2'\psi_{1,2} \pm (c_0/2\Omega R)A_2\dot{y}_{1,2}$$

$$+ (c_0 R/2\Omega R)A_3\dot{\eta}_{1,2}] \tag{24c}$$

$$M_{z_0} = RC[\pm(c_0/2)A_2'\eta_{1,2} \pm (c_0/2\Omega R)A_2\dot{z}_{1,2}$$

$$- (c_0 R/2\Omega R)A_3\dot{\psi}_{1,2}] \tag{24d}$$

where the constants A_1, A_1', A_2, A_2', and A_3 were also obtained in a closed form by Houbolt and Reed in their two-dimensional model.[3] However, note that here

$$y_{1,2} = v_{1,2} + \psi_{1,2}d - h_y \tag{25}$$

$$z_{1,2} = w_{1,2} + h_{1,2} - h_z \pm \theta a + \eta_{1,2}d \tag{26}$$

where, in Eq. (26), the plus sign is carried by the (aj_0) engine

and the minus sign by the $(-aj_0)$ engine. The pusher and tractor versions are naturally identified by the sign of d in Eqs. (25) and (26).

Some Physical Understanding

In Eq. (24a-24d), each aerodynamic influence coefficient $A_1, \ldots, A_3$ has a specific nature concerning its physical background. A brief description of their origin is discussed for the sake of completeness.

Force Coefficients

A_1' and A_1 in the force equations (24a) and (24d) have been known since 1909, when Lanchester discovered that a propeller in yaw develops a side force like that of a fin.[11] Ribner, in a classical paper,[12] demonstrated how to calculate these coefficients by analytical expressions. Houbolt and Reed[3] obtained them by the method described in the present work. Figure 8 displays a side view of the propeller disk and the perturbation lift resultant from either an angular displacement or an induced crossflow generated by the propeller motion relative to the undisturbed flow.

In Eqs. (24a) and (24b), A_2 has quite an interesting meaning. It is an unsteady term originated as a result of summing out the lift lags with respect to the angle of attack over all propeller blades. It appeared in the present formulation without any preestablished unsteadiness assumption. The lag generates a thrust-force component in the propeller plane, which is, of course, dependent upon the direction of the propeller rotation.

Moment Coefficients

Figure 9 explains how coefficients A_2' and A_2 in Eqs. (24c) and (24d) are originated by crossflows due to either an angular displacement or an imparted airspeed in the propeller plane and how they both depend on whether the propeller is spinning clockwise or counterclockwise. The effect of the crossflow is demonstrated in Fig. 7. Keeping the undisturbed velocity vector V constant, a change in the blade angle of attack is obtained by either increasing or decreasing the magnitude of the Ωr vector. In the former case, it corresponds to an increase both in the angle of attack and in the blade lift. Therefore, in the half-portion of the disk where Ωr is in the same direction of the velocity perturbation vector, there is a reduction in the magnitude of Ωr and a decrease in the lift (and thrust). Since the opposite occurs in the other half-portion of the disk, a force couple is generated in a plane normal to the original pertrurbation. The sign of the couple is obviously dependent upon the propeller spinning direction.

Figure 10 explains the derivation of the coefficient A_3. A side view of the propeller disk shows an induced normal airspeed created by an angular-velocity perturbation. This inflow disturbance has different directions in the upper and lower halves of the propeller disk. It adds to the undisturbed airflow in the upper half and subtracts from it in the lower half. A_3 is now associated with the generation of a force couple in the plane of the original perturbation. From Fig. 7, keeping Ωr fixed, a decrease in V leads to an increase in the thrust, which is independent from the propeller spinning direction.

Aeroelastic Stability Equations

Recalling Fig. 3, the virtual work done by the aerodynamic forces is given by

$$\delta W = \sum_i Q_i \delta q_i \tag{27}$$

where

$$Q_1 = M_{z0_1} + L_{y0_1} d, \qquad Q_2 = L_{y0_1}, \qquad Q_3 = -L_{y0_1} - L_{y0_2} \tag{28a-c}$$

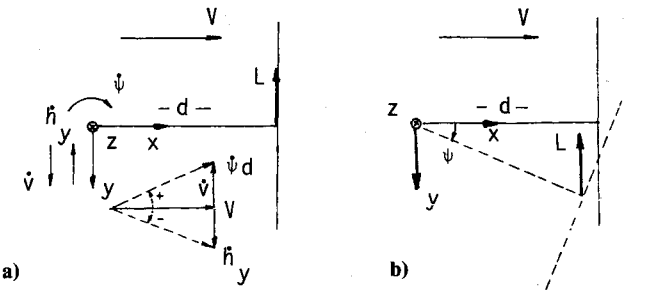

Fig. 8 Aerodynamic influence coefficients: a) A_1 and b) A_1'.

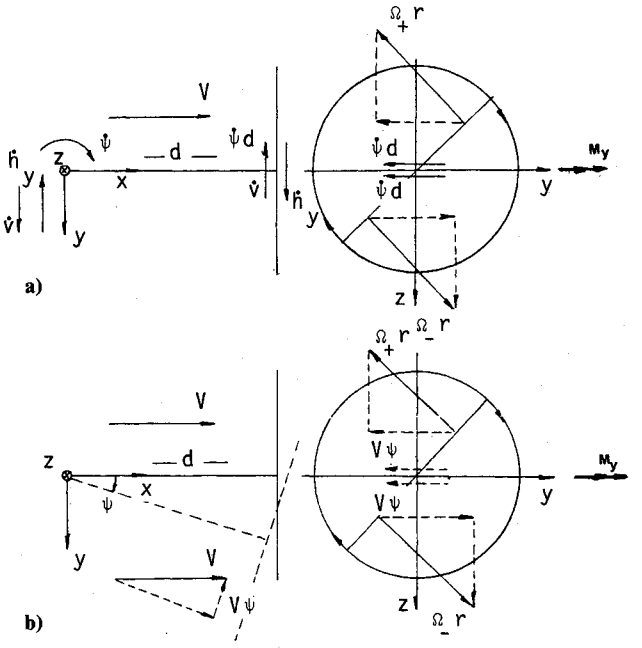

Fig. 9 Aerodynamic influence coefficients: a) A_2 and b) A_2'.

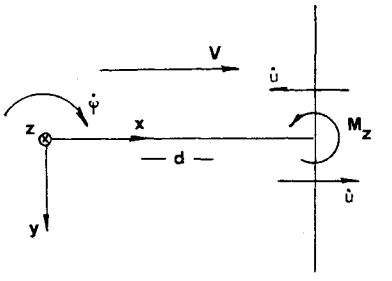

Fig. 10 Aerodynamic influence coefficient A_3.

$$Q_4 = L_{y0_2}, \qquad Q_5 = M_{z0_2} + L_{y0_2} d, \qquad Q_6 = M_{y0_1} - L_{z0_1} d \tag{28d-f}$$

$$Q_7 = Q_6, \qquad Q_8 = L_{z0_1}, \qquad Q_9 = Q_8 \tag{28g-i}$$

$$Q_{10} = -L_{z0_1} - L_{z0_2}, \qquad Q_{11} = a(L_{z0_1} - L_{z0_2}), \qquad Q_{12} = L_{z0_2} \tag{28j-l}$$

$$Q_{13} = Q_{12}, \qquad Q_{14} = M_{y0_2} - L_{z0_2} d, \qquad Q_{15} = Q_{14} \tag{28m-o}$$

and a positive d corresponds to a pusher propeller.

The aeroelastic equations are then obtained via Lagrange equations

$$\frac{d}{dt}\frac{\partial T}{\partial \dot{q}_i} - \frac{\partial T}{\partial q_i} + \frac{\partial E}{\partial q_i} = Q_i \tag{29}$$

where

$$Q_i = \frac{\delta W}{\delta q_i} \tag{30}$$

and are next reduced to their dimensionless form, yielding a system of 15 linear, coupled differential equations, which in the matrix form reads

$$M\overset{**}{q} + (G - \mu Q^1)\overset{*}{q} + (K - \mu Q^0) = 0 \tag{31}$$

where G is skew-symmetric and Q^1 is symmetric. A general comment about the nature of these matrices is presented in the Appendix. The final and straightforward step is to transform the time-dependent problem into the frequency domain by taking, for example, the Laplace transform of Eq. (31). A standard eigenvalue formulation may be obtained by first defining

$$\overset{*}{q} = p \tag{32}$$

and rearranging Eq. (31) as follows:

$$\begin{bmatrix} M & G - \mu Q^1 \\ 0 & 1 \end{bmatrix} \begin{bmatrix} \overset{*}{p} \\ \overset{*}{q} \end{bmatrix} = \begin{bmatrix} 0 & \mu Q^0 - K \\ 1 & 0 \end{bmatrix} \begin{bmatrix} p \\ q \end{bmatrix} \tag{33}$$

Therefore, in the frequency domain, Eq. (33) reads

$$\lambda B\hat{x} = A\hat{x} \tag{34}$$

where λ is the Laplace variable and $\hat{x}$ is the Laplace-transformed vector of the dependent variables

$$\mathcal{L}\lfloor pq \rfloor^T = \hat{x} \tag{35}$$

A computer-library routine is employed to obtain the eigenvalues and eigenvectors of Eq. (34). The eigenvalues of Eq. (34) become all pure imaginary numbers if the aerodynamic stiffness matrix is zeroed, indicating that the whirl-flutter instability is basically originated by the latter matrix, which is proportional to V^2.

Whirl-Flutter Analysis

Figure 11 presents a plot of the dimensionless engine-propeller uncoupled-pitch natural frequency against the whirl-flutter dimensionless parameter $(J/\pi)_c$. A major participation of the backup structure on the system stability is readily noticed. Many different aeroelastic modes are strongly dependent upon $\bar{\omega}_\phi$ and eventually become critical. The corresponding phasor diagrams for these modes are presented in Fig. 12 for the still-air $(J/\pi = 0)$ condition. The propeller hub may precess either in the same or in the opposite direction of the propeller rotation, which is checked by verifying whether the phasor ϕ leads or lags ψ. The former case corresponds to a forward precession if the propeller is spinning clockwise; the latter to a backward precession. For counterclockwise-rotating propellers, a reverse situation is verified. In both cases, the hub motion may be either circular or not. When a simple two-degree-of-freedom model is adopted, the case for which the pitch and yaw stiffnesses are equal $(k_a = 1)$ corresponds to the circular motion. However, if backup structure modes are included the same is no longer true.

The phasor diagrams of Fig. 12 provide a better understanding. Cases for which the mounting system is relatively soft compared to the backup structure correspond to classical whirl-flutter results (cases 1–3). The backup structure is participating in the critical modes, but the major contribution to these modes comes from the familiar hub backward precession. However, much more interesting are the results obtained for higher mounting system stiffness (cases 4–6). The phasor diagrams prove that these modes may not be considered as usual, as they incorporate the motion of an element of the backup structure in a major proportion. Case 4 is typically a transition situation, since the backward precession amplitude is still considerable, but the largest magnitude already corresponds to the pylon symmetric torsion, which is actually complementing the pitch in the propeller precessional motion. Cases 5 and 6 are even more interesting, once the magnitude of the yaw and pitch phasors is negligible and the critical modes may be classified as being respectively: 1) a pylon symmetric bending-torsion plus fuselage vertical bending, and 2) an antisymmetric pylon bending-torsion plus fuselage torsion. The

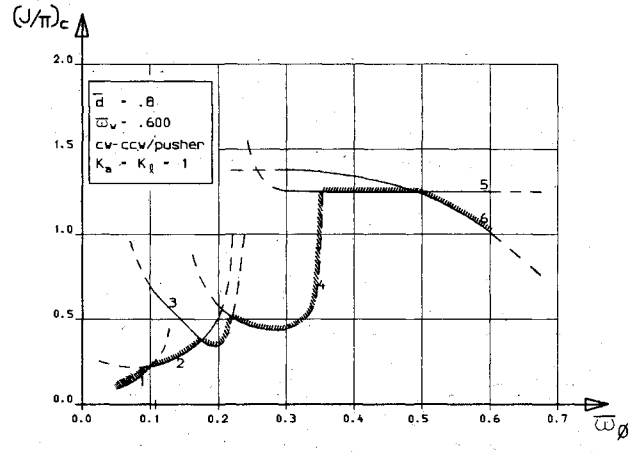

Fig. 11 Whirl-flutter parametric study with dimensionless uncoupled engine-propeller pitch frequency (counter-rotating pusher propellers).

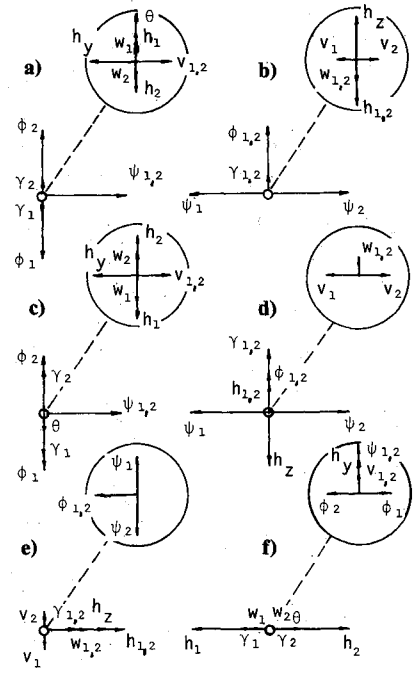

Fig. 12 Phasor diagrams of critical aeroelastic modes for cases 1–6 in Fig. 11. Respectively, from left to right and from top to bottom: a) 1.701 Hz; b) 1.705 Hz; c) 3.851 Hz; d) 7.240 Hz; e) 17.58 Hz; and f) 19.20 Hz.

former mode presents the forward precession, whereas the latter backward.

Since this whirl-flutter-related phenomenon is unusual and perhaps inherent to modern advanced turboprop or propfan installations, it will be called in the present work propeller-whirl-induced backup structure flutter, or shortly *whirl-induced flutter*. It is worth stressing that this kind of flutter is generated only by the propeller aerodynamic and gyroscopic loadings exerted on the backup structure.

A parametric study involving the dimensionless distance $\bar{d}$ between the propeller and the pylon elastic axis is depicted in Fig. 13, where it becomes evident that the pusher propeller (positive values of $\bar{d}$) is more stable than the tractor. Such behavior may be justified by the influence coefficients located close to the diagonal of the aerodynamic stiffness matrix, which are dependent upon $\bar{d}$. When negative, these coefficients decrease the system total stiffness, eventually yielding the divergence condition (curves 1D and 2D in Fig. 13). On the other hand, positive $\bar{d}$ pusher propellers have their stability augmented by the same coefficients. However, the stability is substantially reduced when $\bar{d}$ is small and the off-diagonal coefficients become important.

Six different cases are plotted in Fig. 13 to explore some of the most significant aspects of the present analysis.

Case 1 demonstrates the influence of the relative direction of rotation of the two propellers on the whirl-flutter stability boundaries. From the figure, such influence turns out to be important only for large positive values of $\bar{d}$ (pusher). Indeed, in the tractor version divergence occurred before any difference could develop. The counter-rotating propeller configuration showed to be conservative, once the force and moment perturbations induced by the propeller whirl on both engine suspension systems cancel out in the vertical plane of symmetry of the backup structure.

Case 2 presents a situation for which the global mounting system stiffness is significantly increased. There is a noticeable improvement on the system stability for the tractor installation, although no significant modification was observed in the pusher configuration. There is even a stability drop for very high values of $\bar{d}$. In fact, for such magnitudes of $\bar{d}$ a case of whirl-induced flutter is dominant and the backup structure is already "saturated." Hence, providing the engine installation with a stiffer mounting system is useless to guarantee better stability margins, i.e., the mounting system is working as an dynamic damper, stabilizing the backup structure.

Cases 3–6 help to evaluate the fuselage role on the system stability. It acts as an elastic foundation, damping down the superstructure motion, as long as its resonance frequency is kept within reasonable margins. Case 6 bears the closest resemblence with the classical whirl-flutter problem, as both the pylon and the fuselage are made stiffer and the mounting system softer. In case 5, the backup structure stiffness is maintained at the same levels of case 6, but the engine-mounting system is stiffened a little. Although a traditional whirl-flutter situation is verified, the fuselage is already participating in the stability. The protuberance observed in the curve corresponds to the condition where the fuselage is more efficiently working as a dynamic damper. The overall increase in the stability boundaries is due to the stiffer mounting system, in accordance with a classical whirl-flutter result. In both cases 3 and 4, the pylons are still very stiff to avoid the onset of whirl-induced flutter. The fuselage is, though, softened to the levels of cases 1 and 2. Case 4 is now compared to case 6, as they both have the same engine-mounting system stiffness. In case 4, the stability boundary is higher because the fuselage, being softer, is absorbing more energy from the engine suspension. Likewise, cases 3 and 4 may be compared. Aside from the previous conclusion about the fuselage participation, it is worth observing that in case 3 there is a second protuberance in the stability curve close to the value $\bar{d}=0.6$. This value corresponds to the position where the engine-propeller center of mass is lying on the pylon elastic axis and a decoupling between the pylon and the engine-propeller angular and lateral modes is verified.

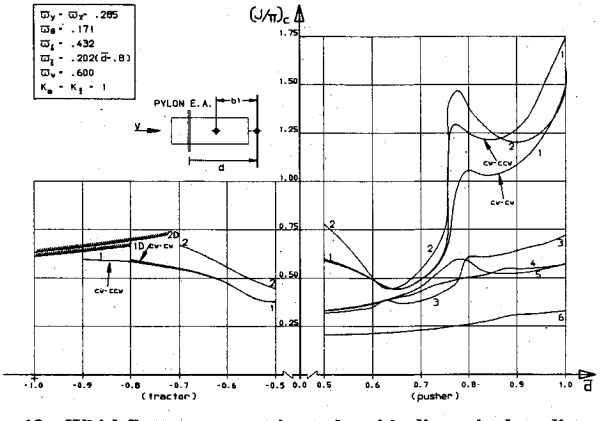

Fig. 13 Whirl-flutter parametric study with dimensionless distance from pylon elastic axis.

Conclusions

The present work stressed the importance of modeling the backup structure in modern configurations of propeller or propfan aircrafts when analyzing the whirl-flutter problem. The model developed may also be directly applied to recent research on vibration insulators, for which two engine-suspension systems are employed: one located at the nacelle-engine interface, and the other at the pylon-fuselage attachment. All of these configurations have in common very flexible backup structures that may flutter in complicated patterns involving the propeller whirl. This new type of flutter was called whirl-induced flutter in the present work. The inclusion of propeller-whirl elements in the detailed aeroelastic analysis of the global aircraft structure seems to be paramount for a reliable analysis.

Appendix: Comments on the Aeroelastic Equations

A general comment on the nature of the matrices defined in Eq. (31) follows from Ref. 10. These matrices may be partitioned in blocks:

$$M = \begin{bmatrix} M_{11} & \\ & M_{22} \end{bmatrix}, \qquad G = \begin{bmatrix} & G_{12} \\ G_{21} & \end{bmatrix}, \qquad G_{12} = -G_{21}^T$$

$$Q^1 = \begin{bmatrix} Q_{11}^1 & Q_{12}^1 \\ Q_{21}^1 & Q_{22}^1 \end{bmatrix}, \qquad Q_{12}^1 = Q_{21}^{1,T}, \qquad Q^0 = \begin{bmatrix} Q_{11}^0 & Q_{12}^0 \\ Q_{21}^0 & Q_{22}^0 \end{bmatrix},$$

$$Q_{12}^0 - Q_{21}^{0\,T}$$

$$K = \begin{bmatrix} K_{11} & \\ & K_{22} \end{bmatrix}$$

where the dependent variables are grouped according to their participation in, respectively, the lateral and vertical motions of the backup structure and engine-support system. Such arrangement provides the minimal band to the above matrices and also seems to be more natural. Hence, the vector of dependent variables yields

$$q_1 = \{\psi_1 \bar{v}_1 \bar{h}_y \bar{v}_2 \psi_2\}$$

$$q_2 = \{\phi_1 \gamma_1 \bar{h}_1 \bar{w}_1 \bar{h}_z \theta \bar{w}_2 \bar{h}_2 \gamma_2 \phi_2\}$$

where the linear-dependent variables are adimensionalized with respect to the propeller radius.

The symmetric mass submatrices are dependent upon the system mass-related properties; namely, masses, c.g. positions, and polar and transverse moments of inertia taken with respect to the pylon elastic axis.

The gyroscopic submatrices are dependent upon both the propeller polar moment of inertia and the respective spinning direction.

The aerodynamic damping submatrices Q^1_{11} and Q^1_{22} are symmetric and dependent upon $\bar{a}$, $\bar{d}$, A_1, and A_3. The off-diagonal submatrix Q^1_{12} is dependent on A_2 and on the spinning direction, akin to G_{12}.

The aerodynamic stiffness submatrices Q^0_{11} and Q^0_{22} are dependent upon $\bar{a}$, $\bar{d}$, and A'_1. As discussed in the main text, these matrices do not have any special property. Finally, the off-diagonal submatrix Q^0_{12} is dependent on A'_2 and also on the propeller spinning direction, as Q^1_{12}.

The dependence of the aforementioned matrices on the spinning direction of propellers 1 (aj_0) and 2 ($-aj_0$) are observed in the sign multiplying, respectively, the upper and lower triangular submatrices obtained by partitioning G_{12}, Q^1_{12}, and Q^0_{12} through their cross diagonals, keeping the original sign for the clockwise rotation and changing the sign for the counterclockwise rotation.

The diagonal structural stiffness matrix K is dependent upon the uncoupled natural frequencies of the engine-mounting system, pylon, and fuselage. All frequencies are adimensionalized by the propeller spinning frequency.

Acknowledgment

The author would like to thank all of EMBRAER's staff for the continuous support to the present investigation. Special thanks are due to the Technical Director, Guido F. Pessoti, whose innovating ideas about aircraft design induced the specialist's work to the present study.

References

[1]Taylor, E. S. and Browne, K. A., "Vibration Isolation of Aircraft Power Plants," *Journal of Aeronautical Sciences*, Vol. 6, No. 2, Dec. 1938, pp. 43–49.

[2]Reed, W. H., III and Bland, S. R., "An Analytical Treatment of Aircraft Propeller Precession Instability," NASA TN D-659, Jan. 1961.

[3]Houbolt, J. C. and Reed, W. H., III, "Propeller-Nacelle Whirl Flutter," *Journal of the Aerospace Sciences*, Vol. 29, March 1962, pp. 333–346.

[4]Zwaan, R. J. and Bergh, H., "Restricted Report F. 228," National Aeronautical Research Institute, NLR, The Netherlands, Feb. 1962.

[5]Sewall, J. L., "An Analytical Trend Study of Propeller-Whirl Instability," NASA TN D-996, April 1962.

[6]Abbot, F. T., Jr., Kelly, H. N., and Hampton, K. D., "Investigation of Propeller-Power-Plant Autoprecession Boundaries for a Dynamic-Aeroelastic Model of a Four-Engine Turboprop Transport Airplane," NASA TN D-1806, April 1963.

[7]Baker, K. E., and Smith, R., and Toulson, K. W., "Notes on Propeller-Whirl Flutter," *Canadian Aeronautics and Space Journal*, Oct. 1965, pp. 305–313.

[8]Reed, W. H., III, "Propeller-Rotor Whirl-Flutter: A State-of-the-Art Review," *Journal of Sound and Vibration*, Vol. 4, No. 3, Nov. 1966, pp. 526–544.

[9]Resende, H. B., "Estudos na Análise de Whirl-Flutter," M.S. Dissertation, Instituto Tecnológico de Aeronáutica, CTA, São José dos Campos, Brazil, 1987.

[10]Nitzsche, F., "Whirl-Flutter Parametric Studies," EMBRAER—Empresa Brasileira de Aeronáutica, São José dos Campos, Brazil, 123-AL-06, Chap. 6, March 1989.

[11]Lanchester, F. W., *The Flying-Machine from an Engineering Standpoint*, Constable & Co. Ltd, London, 1917.

[12]Ribner, H. S., "Propeller in Yaw," NACA Rept. 820, 1945.